University of Bath

Alternative formats
If you require this document in an alternative format, please contact:
openaccess@bath.ac.uk

Compressive behavior of concrete-filled square stainless steel tube stub columns

Peng Dai[1,2a], Lu Yang[*1,2], Jie Wang[3b], Keyang Ning[1,2c] and Yi Gang[1,2d]

[1]*The Key Laboratory of Urban Security and Disaster Engineering of Ministry of Education,*
Beijing University of Technology, Beijing 100124, China
[2]*Beijing Engineering Research Centre of High-rise and Large-span Prestressed Steel Structures,*
Beijing University of Technology, Beijing 100124, China
[3]*Department of Architecture and Civil Engineering, University of Bath, Bath BA2 7AY, UK*

Abstract.   Concrete-filled square stainless steel tubes (CFSSST), which possess relatively large flexural stiffness, high corrosion resistance and require simple joint configurations and low maintenance cost, have a great potential in constructional applications. Despite that the use of stainless steel may result in high initial cost compared to their conventional carbon steel counterparts, the whole-life cost of CFSSST is however considered to be lower, which offers a competitive choice in engineering practice. In this paper, a comprehensive experimental and numerical program on 24 CFSSST stub column specimens, including 3 austenitic and 3 duplex stainless steel square hollow section (SHS) stub columns and 9 austenitic and 9 duplex CFSSST stub columns, has been carried out. Finite element (FE) models were developed to be used in parametric analysis to investigate the influence of the tube thickness and concrete strength on the ultimate capacities more accurately. Comparisons of the experimental and numerical results with the predictions made by design guides ACI 318, ANSI/AISC 360, Eurocode 4 and GB 50936 have been performed. It was found that these design methods generally give conservative predictions to the ultimate capacities of CFSSST stub columns. Improved calculation methods, developed based on the Continuous Strength Method, have been proposed to provide more accurate estimations of the ultimate resistances of CFSSST stub columns. The suitability of these proposals has been validated by comparison with the test results, where a good agreement between the predictions and the test results have been achieved.

Keywords: compressive behavior; Continuous Strength Method; concrete-filled square stainless steel tubes; parametric study; stub column tests

1. Introduction

Concrete-filled stainless steel tubes (CFSST) combines the advantages of both the stainless steel materials and the structural form of concrete-filled steel tubes (CFST), where the former offers high corrosion resistance, low maintenance cost and high ductility (Baddoo 2008, Rossi 2014, Gao *et al*. 2018, Averseng *et al*. 2017) and the latter realizes steel-concrete composite action with high structural efficiency (Zhao 2013, Wang *et al*. 2018, Thomas and Sandeep 2018). Despite that the use of stainless steel may result in high initial cost compared to their conventional carbon steel counterparts, the whole-life cost of CFSST is however considered to be lower, which offers a competitive choice in engineering practice (Lam and Gardner 2008, Uy *et al*. 2011, He *et al*. 2019).

The structural behavior of CFST columns has been widely studied experimentally and numerically, focusing mainly on their static (Sakino *et al*. 2004, Wang *et al*. 2017, Gunawardena *et al*. 2019) and dynamic performance (Huang *et al*. 2018) and bond behavior (Chen *et al*. 2018, Qu *et al*. 2015). However, research works on CFSST members have been rather limited. In the researches on the axial resistance of rectangular and square cold-formed CFSST stub columns (Young and Ellobody 2006, Ellobody and Young 2006) and square and circular CFSST stub columns (Lam and Gardner 2008, Uy *et al*. 2011), current codified design rules have been assessed and modified correspondingly. In particular, Lam and Gardner (2008) proposed design equations for the axial resistance of specimens based on the Continuous Strength Method considering the significant material strain-hardening of stainless steels. Investigations in other structural aspects of CFSST focused on their bond (Tao *et al*. 2016), hysteretic (Liao *et al*. 2017), flexural (Chen *et al*. 2017) and fire-resisting behaviors (Han *et al*. 2013). There have also been studies on CFSST members filled with recycled aggregate concrete (Yang and Ma 2013, Tam *et al*. 2014) and seawater and sea sand concrete (Li *et al*. 2016a, b).

It is worth noting that previous research on concrete-filled stainless steel tube has been limited to cold-formed thin-walled tubes, whereas hot-rolled tubes have been rarely unexplored (Dai *et al*. 2020). Hot-rolled stainless steel tubes generally have larger wall thicknesses and more

homogeneous material properties than cold-formed members, thereby offering improved structural stability and ductility (Gardner *et al*. 2010) and providing greater constraint on core concrete. Furthermore, there is no systematic design formula for the axial ultimate bearing capacity of CFSST members, and their design in engineering practice mainly refers to the design codes for CFST members, which require further study to verify their applicability.

In the current work, an experimental program was carried out to analyze the compressive behavior of CFSSST stub columns with hot-rolled tubes. Square cross-sections were chosen as they have simpler joint configurations and larger cross-section modulus than circular ones (Wang *et al*. 2019). A total of 24 axial compressed specimens, comprising 6 square hollow section (SHS) tubes and 18 CFSSST stub columns, were tested. FE models were developed to duplicate the tests and further utilized in a large-scale parametric study considering concrete strengths and cross-sectional geometries. Based on the test and numerical results, calculation formulas for the axial resistance of CFSSST stub columns were put forward in light of the existing design codes ACI 318 (2011), ANSI/AISC 360 (2010), BS EN 1994-1-1 (2004) and GB 50936 (2014).

2. Experimental program (Dai *et al*. 2019)

2.1 General

In the experimental program of the current study, 24 stub column tests were performed to investigate the ultimate compressive capacities of CFSSST cross-sections. Material

tests were also conducted for the analyses of the stub column test results and to be used in the subsequent numerical study.

Table 1 provides a list of the stub column specimens, including 6 square hollow section (SHS) tubes and 18 CFSSST stub columns. The stub column specimens covered two steel grades (Grades 304 and S32205 according to ASTM A959 (2009)), three steel cross-section geometries (SHS 296×296×8, 300×300×10 and 304×304×12) and three concrete grades (C50, C70 and C80). All the specimens were designed to have a nominal height of 840 mm. In Table 1, the first letter "A" or "D" in the specimen label designation denotes the austenitic and duplex stainless steel grades respectively, the "t8", "t10" or "t12" refers to the nominal wall thickness of 8, 10 or 12 mm, the "C50", "C70" or "C80" represents the concrete grade, and the "SHS" refers to the pure steel SHS stub columns without the concrete core.

The 0.2% proof strength ($f_{0.2}$) of the stainless steel and the cube compressive strength (f_{cu}) of the concrete were acquired from the material tests detailed in Section 2.3, and ξ is the confinement factor $\xi = A_s f_{0.2}/A_c f_{ck}$ (Han *et al*. 2005), with A_s and A_c being the cross-section areas of the tube and concrete, respectively, and f_{ck} being calculated as $0.67 f_{cu}$ according to BS EN 1992-1-1 (2004).

2.2 Specimen preparation

The manufacturing process of the CFSSST specimens is demonstrated in Fig. 1. The tubes were firstly built-up by welding four austenitic (or duplex) stainless steel plates together to form the box-section geometry. Two Q235 carbon structural steel end plates were then welded to both sides of the stainless steel tubes. Prior to welding the second

Table 1 Measured dimensions, material properties and ultimate capacities of test specimens

Specimen	B (mm)	t (mm)	L (mm)	$f_{0.2}$ (MPa)	f_{cu} (MPa)	ξ	N_{exp} (kN)
A-t8C50	295.50	7.75	839.80	293	48.2	1.10	6290
A-t10C50	299.74	9.87	839.70	287	48.2	1.36	7113
A-t12C50	303.74	11.87	842.00	301	48.2	1.72	7924
A-t8C70	295.50	7.75	840.30	293	71.7	0.76	6743
A-t10C70	299.74	9.87	840.10	287	71.7	0.93	7947
A-t12C70	303.74	11.87	840.00	301	71.7	1.18	8575
A-t8C80	295.52	7.76	840.50	293	82.1	0.67	7436
A-t10C80	299.72	9.86	839.30	287	82.1	0.82	8430
A-t12C80	303.70	11.85	840.10	301	82.1	1.04	9257
A-t8-SHS	295.56	7.78	840.60	293	-	-	2340
A-t10-SHS	299.68	9.84	838.90	287	-	-	3257
A-t12-SHS	303.66	11.83	841.40	301	-	-	4495
D-t8C50	295.76	7.88	840.20	634	48.2	2.38	8771
D-t10C50	299.60	9.80	840.50	590	48.2	2.79	10111
D-t12C50	304.98	12.49	839.50	576	48.2	3.29	12472
D-t8c70	295.72	7.86	840.70	634	71.7	1.64	9686
D-t10C70	299.66	9.83	841.00	590	71.7	1.92	10820
D-t12C70	305.00	12.50	839.30	576	71.7	2.27	12560
D-t8C80	295.70	7.85	840.40	634	82.1	1.45	9962
D-t10C80	299.86	9.93	842.20	590	82.1	1.69	11728
D-t12C80	304.92	12.46	840.10	576	82.1	2.00	13272
D-t8-SHS	295.64	7.82	839.10	634	-	-	3643
D-t10-SHS	299.88	9.94	842.10	590	-	-	5671
D-t12-SHS	304.80	12.40	841.10	576	-	-	8238

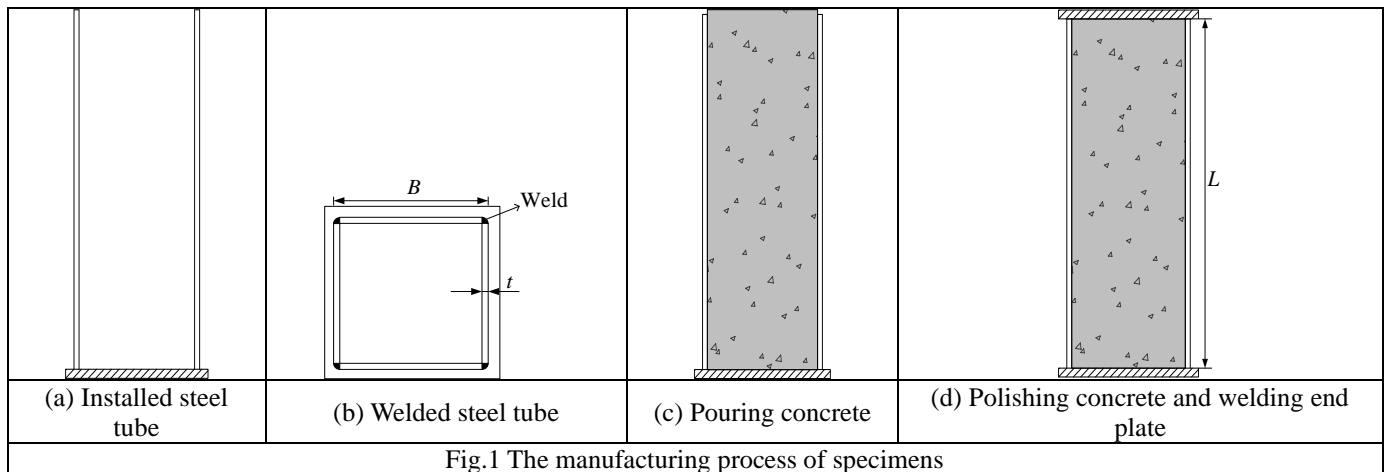| (a) Installed steel tube	(b) Welded steel tube	(c) Pouring concrete	(d) Polishing concrete and welding end plate
Fig.1 The manufacturing process of specimens			

Table 2 Mechanical properties of stainless steel tubes

Steel grade	t (mm)	$\sigma_{0.01}$ (Mpa)	$\sigma_{0.2}$ (Mpa)	σ_u (Mpa)	E_0 (Mpa)	ε_u (%)	ε_f (%)	n
	8	204	293	692	196603	44.2	51.5	6.5
304	10	193	287	697	196206	43.6	52.2	6.1
	12	222	301	661	199393	46.3	56.8	6.0
	8	527	634	808	198167	15.4	29.4	6.8
S32205	10	484	590	784	198778	18.8	34.1	6.6
	12	434	576	745	195035	19.0	37.7	6.4

end plate, concrete was poured into the steel tube in layers and fully vibrated to ensure compactness. After 28 days of natural curing, the concrete surface slightly exceeded the upper surface of the steel tube. Therefore, the concrete was polished until it ended at the same height as the end section of tube, enabling the second end plate to be welded to the steel tube.

2.3 Material properties

For each stainless steel cross-section (two steel grades and three cross-section sizes), three coupons were extracted. The sizes of the coupons varied for different tube thicknesses, as detailed in Fig. 2. All the tensile coupon tests were conducted in the light of BS EN ISO 6892-1 (2009). Typical obtained stress-strain curves of the stainless steel are given in Fig. 3. The averaged material properties are reported in Table 2, where $\sigma_{0.2}$ are the 0.2% proof strength, σ_u are ultimate strength, ε_u and ε_f are the strain at the ultimate stress and percentage elongation after fracture, respectively, E_0 is the initial elastic modulus, and n is the strain hardening exponent according to the R-O model (BS EN 1993-1-4 2015).

The concrete strength for C50, C70 and C80 concrete were obtained from concrete cube tests. For each concrete grade, three 100 mm cubes were cast and cured in same environment with the corresponding batch of concrete in CFSSST. These cubes were tested subjected to compression at 28 days of curing to obtain f_{cu} of the concrete. The averaged cube compressive strengths are given in Table 1 and the proportions of the concrete mix are detailed in Table 3.
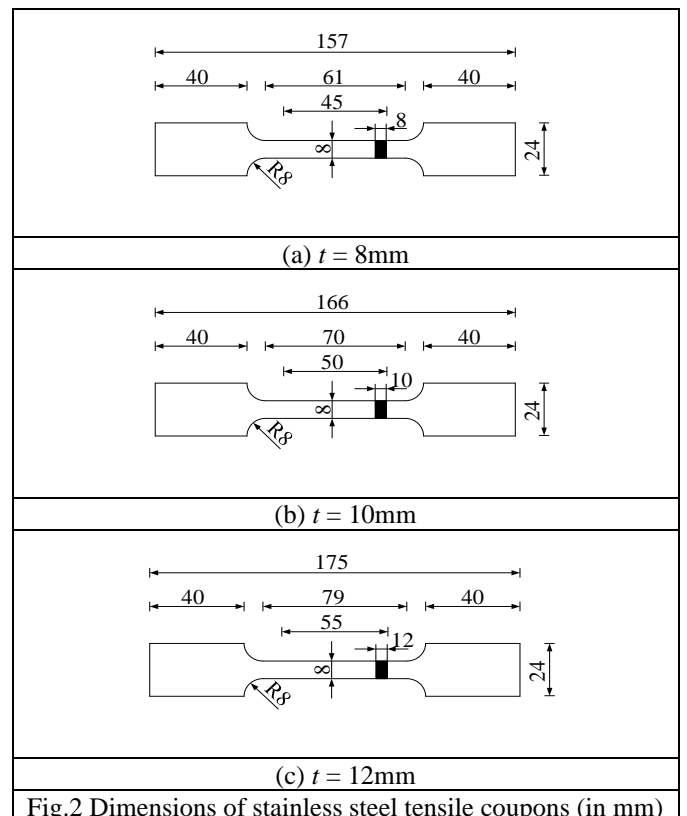

(a) $t = 8$mm

(b) $t = 10$mm

(c) $t = 12$mm

Fig.2 Dimensions of stainless steel tensile coupons (in mm)

(a) *t* = 8mm

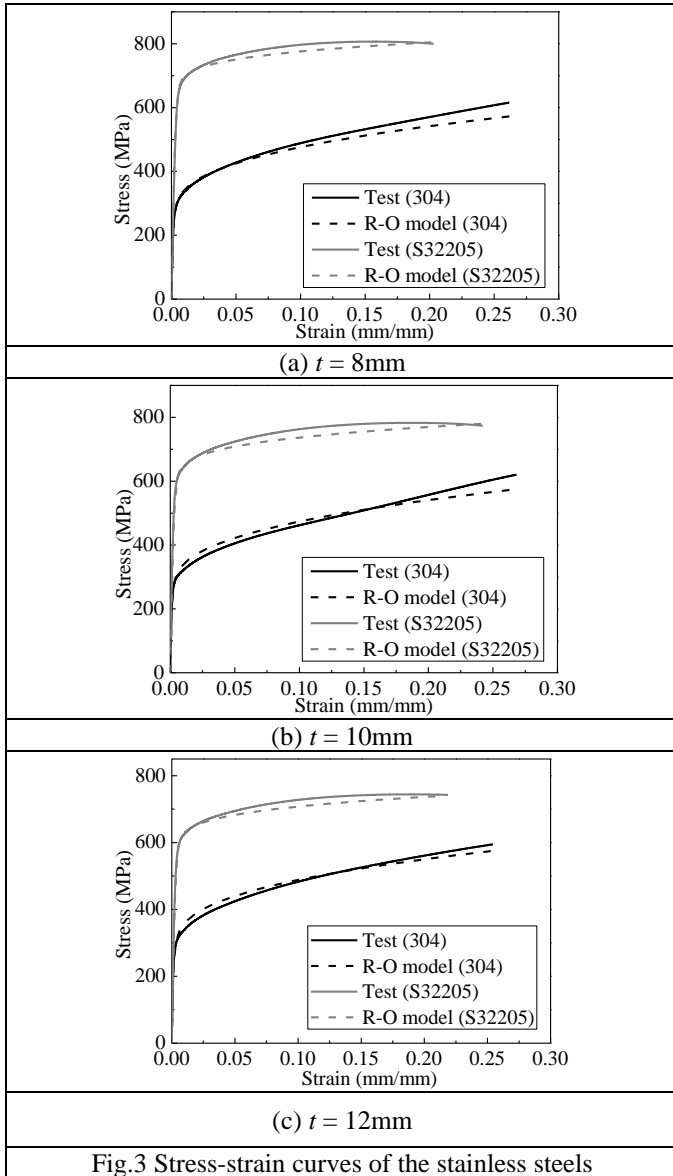(b) *t* = 10mm

(c) *t* = 12mm

Fig.3 Stress-strain curves of the stainless steels
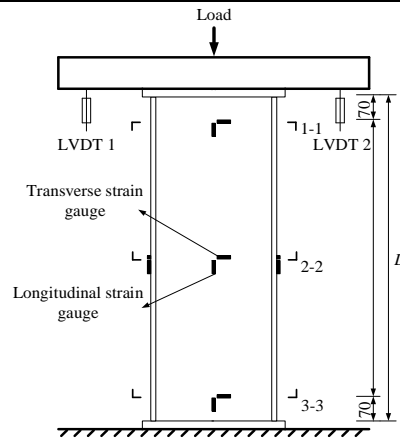
2.4 Stub column test setup

The test setup of stub columns was shown in Figs. 4(a) and (b), respectively. The CFSSST and stainless steel SHS stub columns were fixed supported at both ends. The compressive load was applied through the vertical movement of the top loading head.

The instrumentations of the stub column tests are detailed in Fig. 4(b), where two linear variable displacement transducers (LVDT1 and LVDT2) were arranged diagonally at the top loading plate to measure the longitudinal shortening, and transverse and longitudinal strain gauges were affixed at the middle height section (Fig. 4(c)) and at the top and bottom sections (70 mm away from the end plate, Figs. 4(d)-(e)) of the tubes to record their strain development. It should be noted that the longitudinal strain gauge readings indicated the development of the axial shortening, buckling and eccentricity, whilst the transverse strain gauges monitored the distribution of strain before and after buckling of the tube and the constraint of the stainless steel tube to the concrete. In the strain gauge designation in Figs. 4(c)-(e), "SG" denotes the strain gauges, the first number 1, 2 or 3 represents the sections 1-1, 2-2 and 3-3 of the specimen in Fig. 4(b), respectively, the second number 1, 2 and 3, 4 indicate the longitudinal strains and the transverse strains, respectively, and for the section 2-2 in Fig. 4(b), SG2-1 to 4 are the longitudinal and SG2-5 to 8 are the transverse strain gauges, respectively.

All the stub column tests were applied to the displacement with a rate of 1 mm/min and terminated when the load dropped to approximately 75% of the peak load, at which obvious local buckling of the tube had generally been observed. The load eccentricities were derived from the longitudinal strain gauge readings at section 1-1 (Fig. 4(b)). The maximum calculated eccentricity was less than 2 mm, which has been verified in the later numerical study to have little effect on the ultimate resistance and failure modes of the CFSSST stub columns.

(a) Photo of test set-up
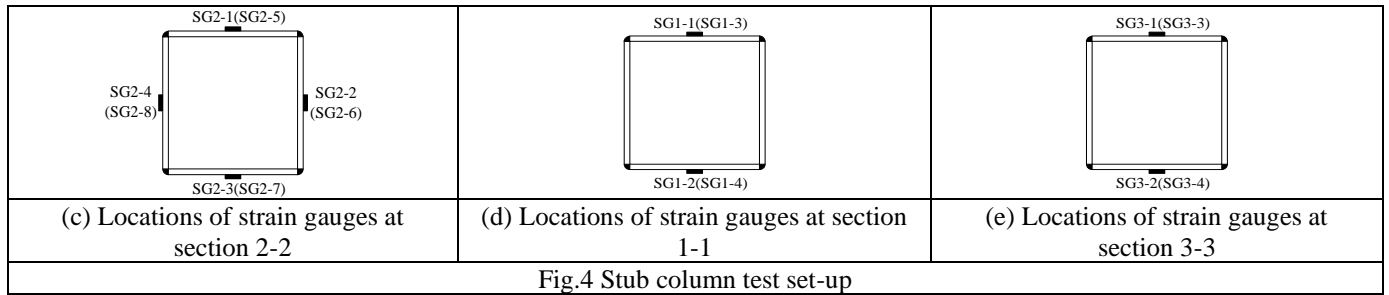

(b) Schematic view of test set-up

(c) Locations of strain gauges at section 2-2	(d) Locations of strain gauges at section 1-1	(e) Locations of strain gauges at section 3-3
Fig.4 Stub column test set-up		

Table 3 Composition of concrete mix (kg/m^3)

Grade	Cement	Water	Sand	Coarse aggregate	Fly ash	Slag	Admixtures
C50	235	165	689	1123	103	74	7.10
C70	307	158	627	1164	93	65	8.13
C80	433	150	550	1168	87	58	10.38

2.5 Test results and discussion

Typical deformed shapes of the stub column specimens and the crushed core concrete are illustrated in Figs. 5 and 6, respectively, and the load-axial deformation relationships are given in Fig. 7. The CFSSST stub columns generally experienced similar failure modes, where the steel tube started to show significant buckling bulges when the load dropped to approximately 80% to 90% of the peak load (see Fig. 7).

The failure modes of all the tested CFSSST stub columns featured out-ward local buckling of the outer tube at approximately the mid-height of the specimens. Some specimens displayed a weld crack following the buckling deformation, as marked in red circles in Fig. 5, which may be caused by two reasons: 1) the position of the weld seam was at the corner region of the square steel tube, which had larger transverse stresses than at the flat regions; 2) welding defects may be generated during the manufacturing process of the CFSSST specimens. It should be noted that the buckling waves in the CFSSST specimens were all in the convex direction whereas the empty stainless steel SHS specimens displayed a typical plate local buckling mode with a combination of both convex and concave surfaces, as shown in Fig. 5, indicating the significant influence of concrete core on the buckling deformation of the stainless steel tubes. In addition, the failure mode of the core concrete was associated with complete crush of the concrete at the position where the stainless steel tubes buckled, as shown in Fig. 6. It indicates that the stainless steel tube in turn had a restraining influence on concrete core.
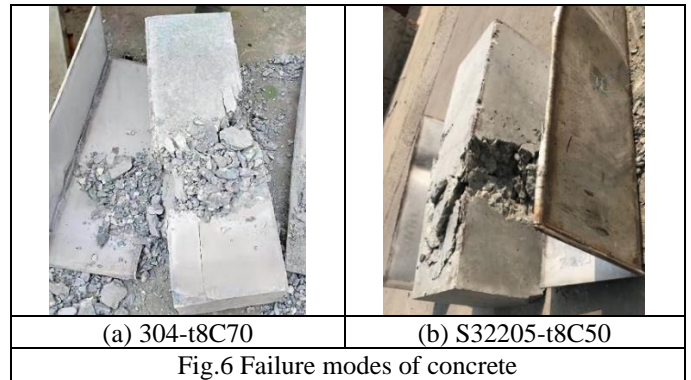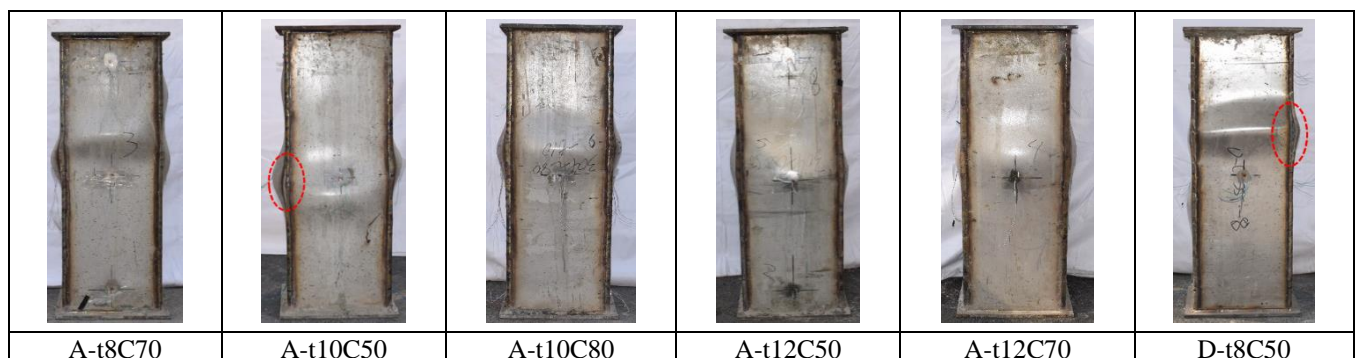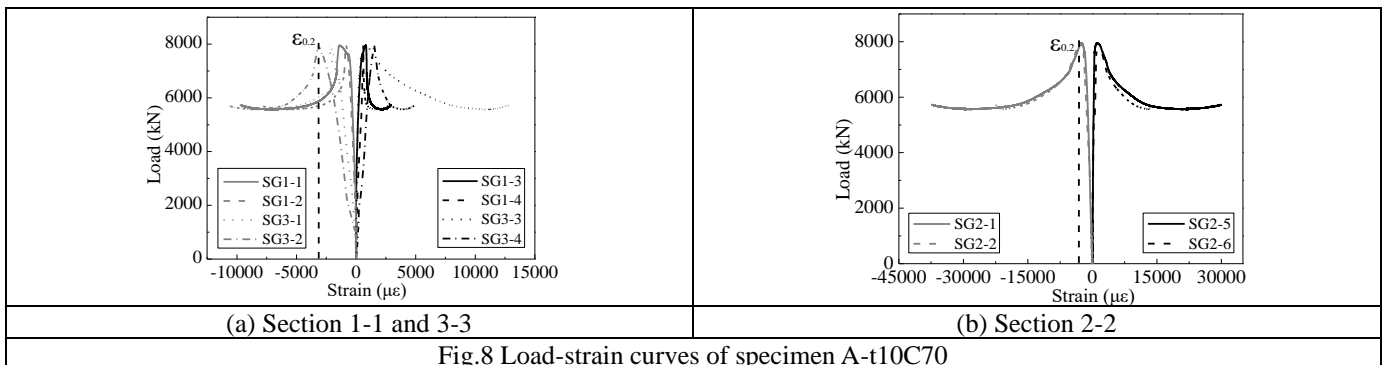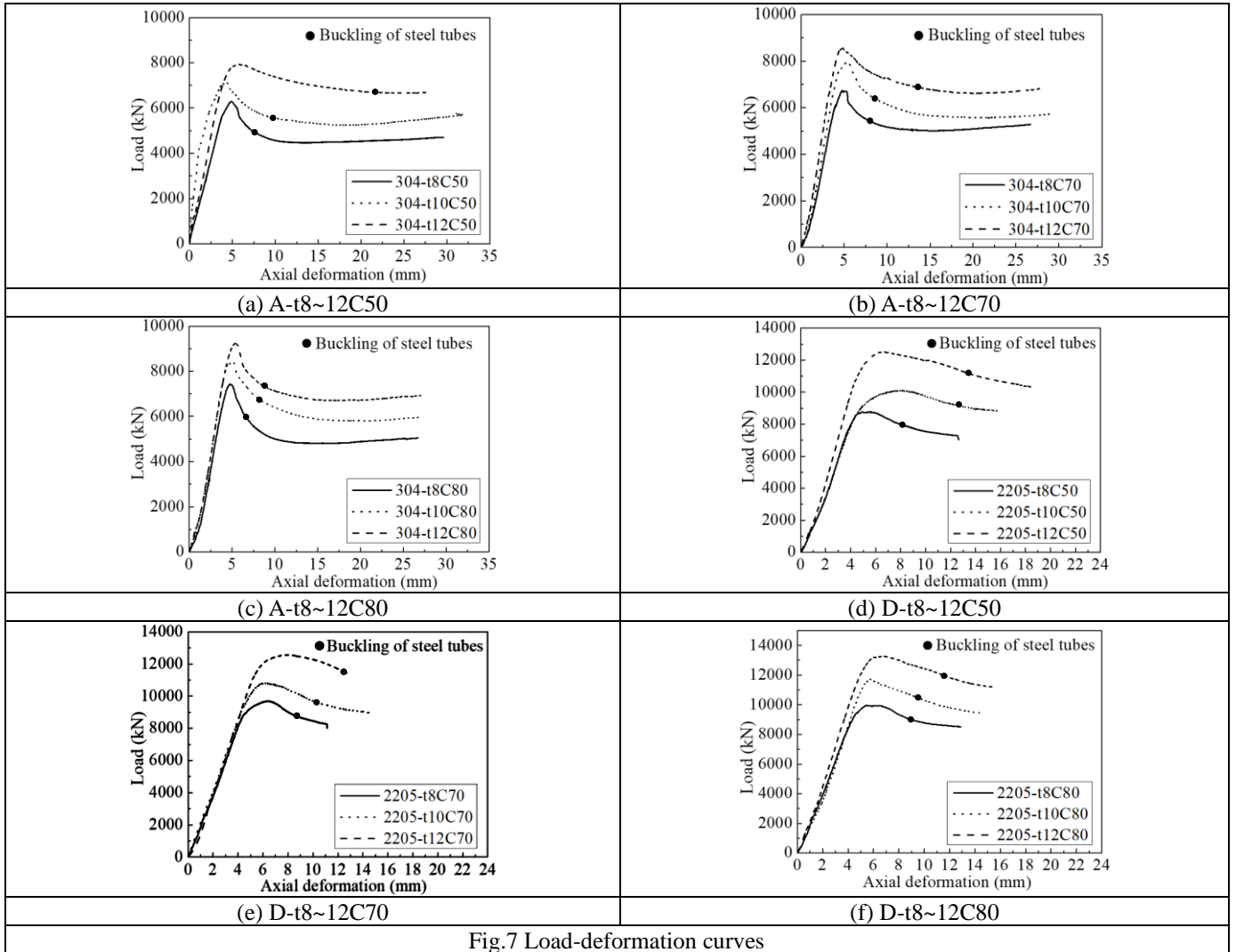

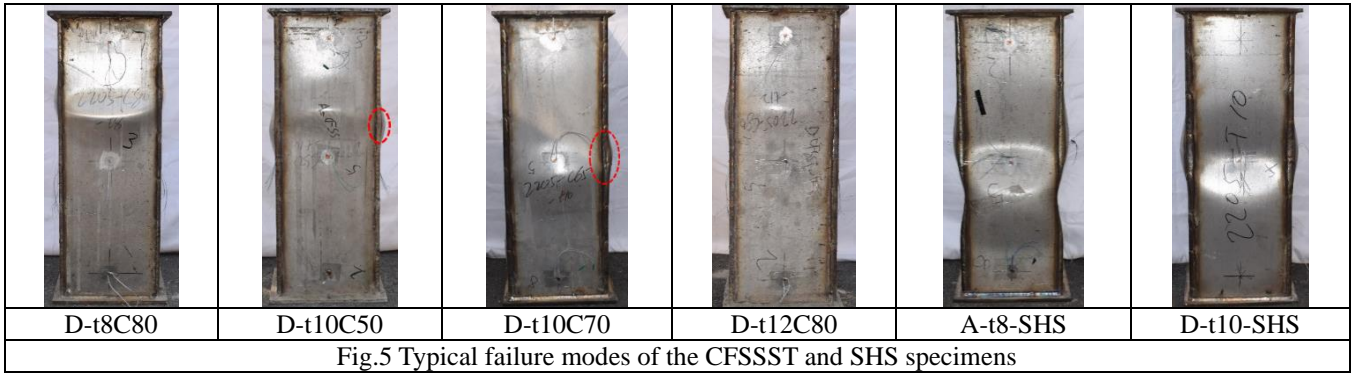| (a) 304-t8C70	(b) S32205-t8C50
Fig.6 Failure modes of concrete	

As expected, the ultimate capacities (peak loads achieved in the tests) of the CFSSSTs are greatly influenced by wall thickness of the steel tube and the concrete grade as shown in Fig. 7. During the tests, after the peak load was reached, the load application was paused at every 3 mm increase of the axial displacement to observe whether the tube had buckled. The black dots marked on the load-axial deformation curves in Fig. 7 represent the moment when significant steel tube buckling occurred. It can be found that the CFSSSTs with larger steel tube wall thicknesses can resistance larger axial deformation before buckling. It should be noted that after the steel tube buckled, the austenitic specimens generally displayed a slowly onset of

A-t8C70	A-t10C50	A-t10C80	A-t12C50	A-t12C70	D-t8C50

| D-t8C80 | D-t10C50 | D-t10C70 | D-t12C80 | A-t8-SHS | D-t10-SHS |

Fig.5 Typical failure modes of the CFSSST and SHS specimens

(a) A-t8~12C50

(b) A-t8~12C70

(c) A-t8~12C80

(d) D-t8~12C50

(e) D-t8~12C70

(f) D-t8~12C80

Fig.7 Load-deformation curves

(a) Section 1-1 and 3-3

(b) Section 2-2

Fig.8 Load-strain curves of specimen A-t10C70

load bearing capacity (Figs. 7(a)-(c)), whereas this phenomenon did not appear in the duplex specimens (Figs. 7(d)-(f)). This may be attributed to the facts that 1) the austenitic steel (304) possesses higher material strain-hardening than the duplex steel (S32205), and 2) the duplex steel tubes with higher yield strength have higher normalized slenderness for the same cross-section geometry compared to their austenitic counterparts.

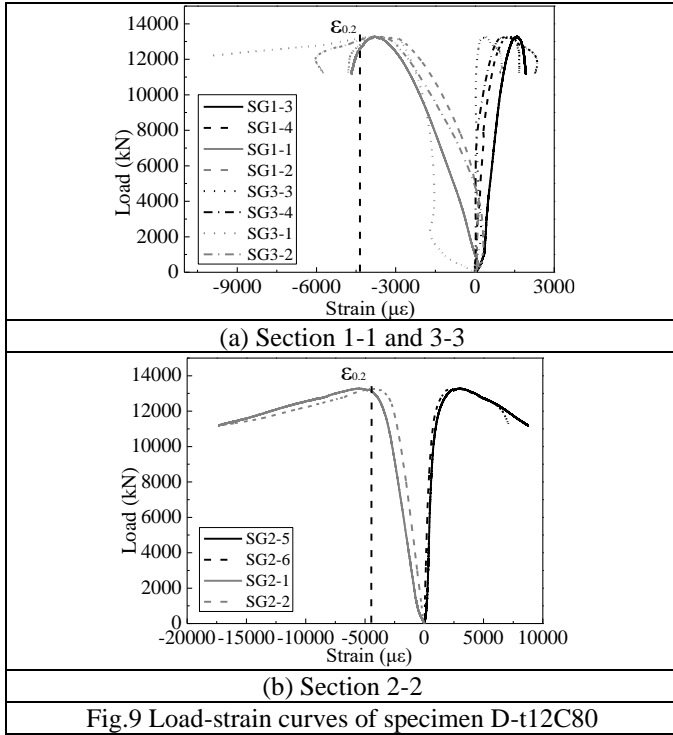(a) Section 1-1 and 3-3

(b) Section 2-2

Fig.9 Load-strain curves of specimen D-t12C80

The strain development in typical 304 and S32205 CFSSST members are shown in Figs. 8 and 9 respectively, where two longitudinal and two transverse strain gauge readings at each section height (section 1-1, 2-2 and 3-3 in Fig. 4(b)) are plotted. The vertical dashed lines in Figs. 8 and 9 represent the yield strains $\varepsilon_{0.2}$ (at $\sigma_{0.2}$) of the corresponding stainless steel tubes. The longitudinal strains of these two specimens at all section heights generally did not exceed the $\varepsilon_{0.2}$ at the peak load, indicating that the failure in these two specimens was caused by the crush of the core concrete. However, this was not the case for all the specimens. Fig. 10 plot the averaged longitudinal strain gauge readings, ε_{ult}, at the mid-height section (section 2-2) for all the specimens, where the yield strains, $\varepsilon_{0.2}$, are also drawn for comparison purpose. It shows that the specimens with lower concrete grades and higher tube thicknesses experienced steel tube yielding at failure.

In Fig. 10, as the concrete grade increases, the averaged compressive longitudinal strain at the ultimate load, ε_{ult}, decreases. It may be due to the fact that higher concrete grade is associated with higher elastic modulus, hence can result in a reduced overall strain of the CFSSST specimen at failure. For specimens with the same concrete grade, the thicker the stainless steel tube, the higher the overall strain at failure, which was simply because the specimens with thicker steel tubes can resist higher deformation before
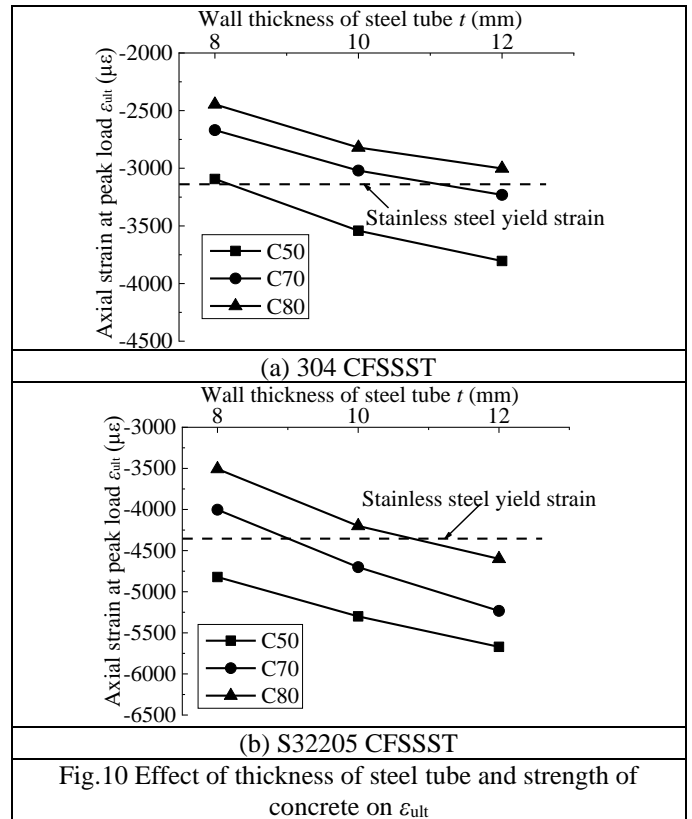
failure occurs.

(a) 304 CFSSST

(b) S32205 CFSSST

Fig.10 Effect of thickness of steel tube and strength of concrete on ε_{ult}

3. Numerical modelling

3.1 Overview

In parallel to the tests, a numerical study was conducted to study the compressive performance of CFSSST stub columns by using the FE analysis ABAQUS software. The FE modelling details, including the constitutive models of the stainless steels and the core concrete, surface contact, boundary conditions, load application and mesh, are reported in this section.

3.2 Material modelling of stainless steel tubes

The stress-strain relationships used in the FE models were defined according to (Ramberg and Osgood 1943, Mirambell and Real 2000, Rasmussen 2003) as shown in Eq. (1), where the key parameters were based on the corresponding tensile coupon test results as reported in Table 2, including the strain hardening exponent $n = \ln(20)/\ln(\sigma_{0.2}/\sigma_{0.01})$, being $\sigma_{0.01}$ the measured 0.01% proof stress, the tangent elastic modulus $E_{0.2}$ at the moment when the stress reaches $\sigma_{0.2}$, and the coefficient m calculated as $m = 1+3.5\sigma_{0.2}/\sigma_u$.

It should be noted that Eq. (1) represents only the engineering stress-strain relationship as measured from the tensile coupon tests, which does not take the instantaneous reduction of the coupon's cross-section area into account.

Therefore, the true stress-strain relationships employed in the FE models can be obtained from the engineering stress-strain relationships built up using Eq. (1), as below:

$$\varepsilon=\begin{cases} \dfrac{\sigma}{E_0}+0.002(\dfrac{\sigma}{\sigma_{0.2}})^n & (\sigma \leq \sigma_{0.2}) \\ \dfrac{\sigma-\sigma_{0.2}}{E_{0.2}}+\varepsilon_u(\dfrac{\sigma-\sigma_{0.2}}{\sigma_u-\sigma_{0.2}})^m+\varepsilon_{0.2} & (\sigma > \sigma_{0.2}) \end{cases} \quad (1)$$

$$\sigma_{true}=\sigma_{nom}(1+\varepsilon_{nom}) \quad (2)$$

$$\varepsilon_{ln}^{pl}=\ln(1+\varepsilon_{nom})-\sigma_{true}/E_0 \quad (3)$$

where σ_{true} and σ_{nom} are the true and measured engineering stresses, respectively, ε_{ln}^{pl} and ε_{nom} are the true log plastic strain and measured engineering strains, respectively.

3.3 Material modelling of concrete

The elastic behavior of the concrete was defined with a Poisson's ratio of 0.2 and a modulus of elasticity $E_c = 4700(f_c')^{0.5}$ (ACI 318 2011), with f_c' being the cylinder compressive strength of concrete. The plasticity of the concrete comprised of the definitions of the concrete damage plasticity (CDP) and the compressive and tensile stress-strain relationships. The CDP model provided in ABAQUS was employed, with the key parameters set the same as those adopted in a similar study (Tao *et al.* 2013), including the dilation angle ψ of 30 deg, the flow potential eccentricity e of 0.1, the ratio of the compressive strength under biaxial loading to uniaxial compressive strength f_{b0}/f_c' of 1.16, the ratio of the second stress invariant on the tensile meridian to that on the compressive meridian K_c of 2/3 and the viscosity parameter of 0.0001. The compressive σ-ε relationship of concrete core adopted the model proposed by Han *et al.* (2005), which considers the ξ. The tensile σ-ε relationship of the core concrete was defined according to GB 50010 (2010). The specific formulas for compressive and tensile stress-strain relationships are given by Eqs. (4) and (5), respectively.

$$y=\begin{cases} 2x-x^2 & (x \leq 1) \\ \dfrac{x}{\beta_0(x-1)^n+x} & (x > 1) \end{cases} \quad (4)$$

where $x = \varepsilon/\varepsilon_0$, $y = \sigma/f_c'$, $\varepsilon_0 = (1300+12.5f_c'+800\xi^{0.2})\times10^{-6}$; $\beta_0 = (f_c')^{0.1}/(1.2(1+\xi)^{0.5})$; $n=1.6+1.5/x$.

$$y=\begin{cases} 1.2x-0.2x^6 & (x \leq 1) \\ \dfrac{x}{0.31\sigma_p^2(x-1)^{1.7}+x} & (x > 1) \end{cases} \quad (5)$$

where $x = \varepsilon_t/\varepsilon_p$, $y = \sigma_t/\sigma_p$, $\varepsilon_p = 43.1\sigma_p$ ($\mu\varepsilon$), $\sigma_p = 0.26(1.25 f_c')^{2/3}$.

3.4 Surface contact, boundary conditions, load application and mesh

The surfaces between the tube and concrete core, and concrete core with the end plates, adopted a hard contact in normal direction, ensuring that the normal pressure can be completely transferred and the surfaces were allowed to be separated when there is no compressive pressure. In the tangential direction, the friction model was used. For the CFSSST stub columns in the present study, there was almost no sliding between stainless steel tube and concrete. Hence the test results are little affected by the friction coefficient, which is set equal to 0.25 herein following the recommendation in Tao *et al.* (2013).

The two end plates were tied to the end-sections of the stainless steel tube (Ding *et al.* 2019). The top and bottom end plates only release the axial degree of the top end plate. The axial load was applied through a reference point which was located at the centroid of and coupled to the top end plate. The C3D8R was used to model the steel tubes, the core concrete and the bottom and top end plates of the stub columns, respectively. It can be concluded from a mesh sensitivity study that an element size of 10 mm guarantees an error less than 1%. Fig. 11 shows the mesh detail of a typical CFSSST model.
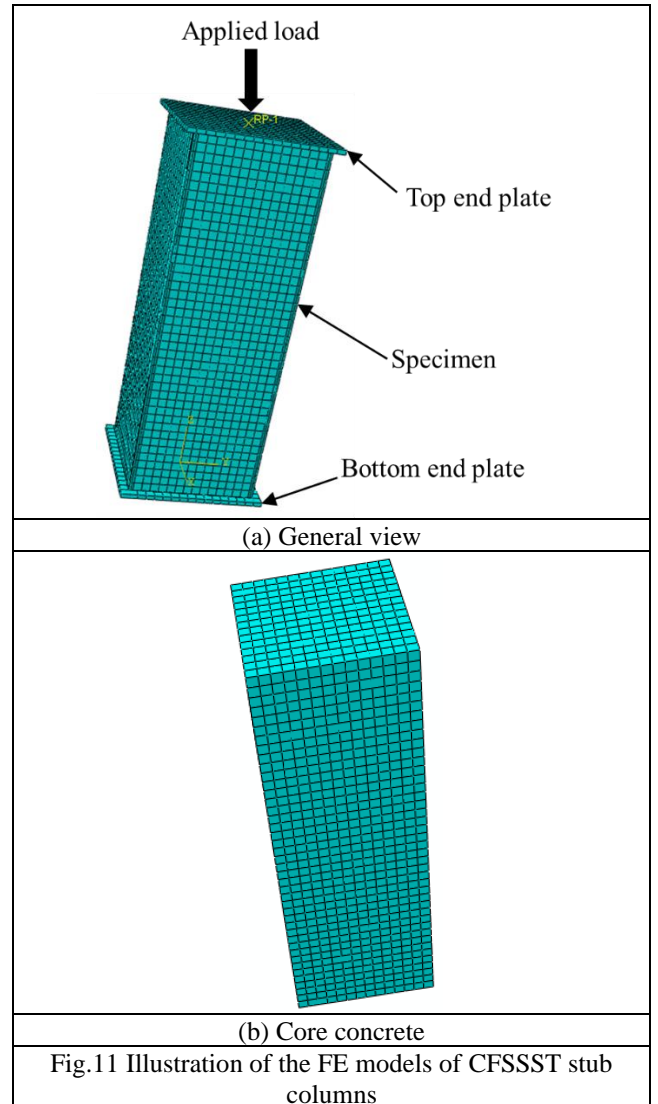

(a) General view

(b) Core concrete

Fig.11 Illustration of the FE models of CFSSST stub columns

Table 4 Comparison of FE and test ultimate loads

Specimen	N_{exp} (kN)	N_{FE} (kN)	N_{FE}/N_{exp}
A-t8C50	6290	6150	0.98
A-t10C50	7113	6780	0.95
A-t12C50	7924	7812	0.99
A-t8C70	6743	7130	1.06
A-t10C70	7947	8150	1.02
A-t12C70	8575	9329	1.09
A-t8C80	7436	8151	1.10
A-t10C80	8430	8878	1.05
A-t12C80	9257	9971	1.08
		Mean	1.04
		COV	0.048
D-t8C50	8771	9272	1.06
D-t10C50	10111	10448	1.03
D-t12C50	12472	11955	0.96
D-t8C70	9686	10824	1.12
D-t10C70	10820	11490	1.06
D-t12C70	12560	13448	1.07
D-t8C80	9962	11002	1.10
D-t10C80	11728	12502	1.07
D-t12C80	13272	13990	1.05
		Mean	1.06
		COV	0.040

(a) Test	(b) FE model

Fig.13 Comparison of test and FE failure modes of specimen A-t10C80

(a) Test	(b) FE model

Fig.14 Comparison of test and FE failure modes of specimen D-t10C50

(a) Austenitic CFSSSTs	(b) Duplex CFSSSTs

Fig.12 Comparison of experimental and FE load-axial deformation curves of typical specimens
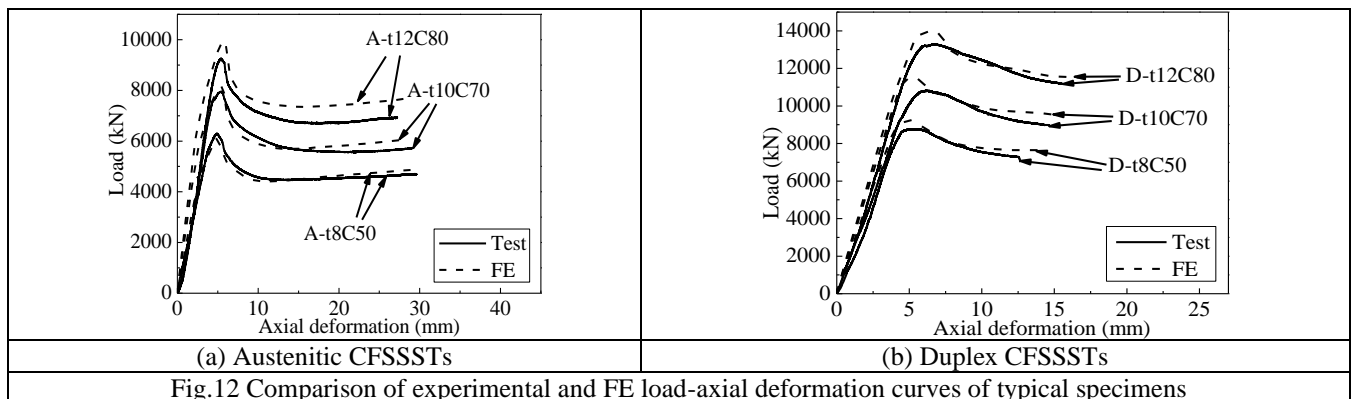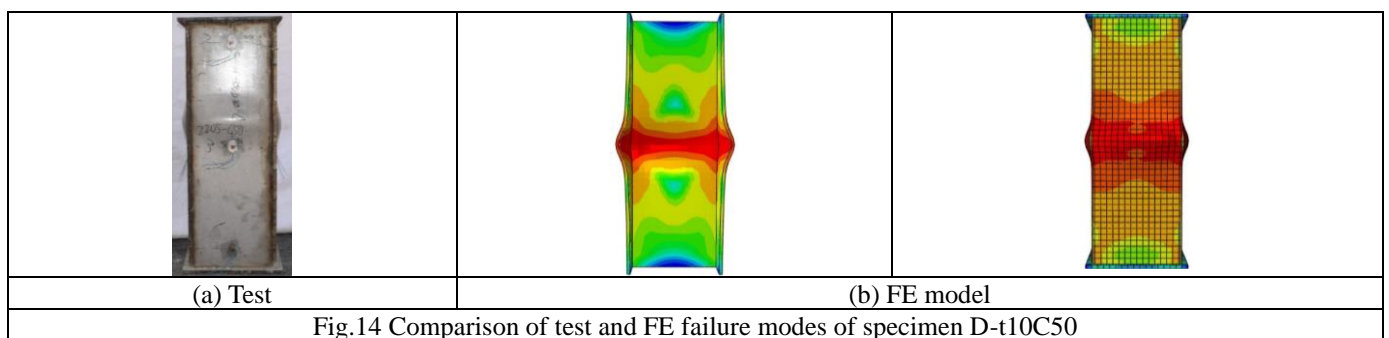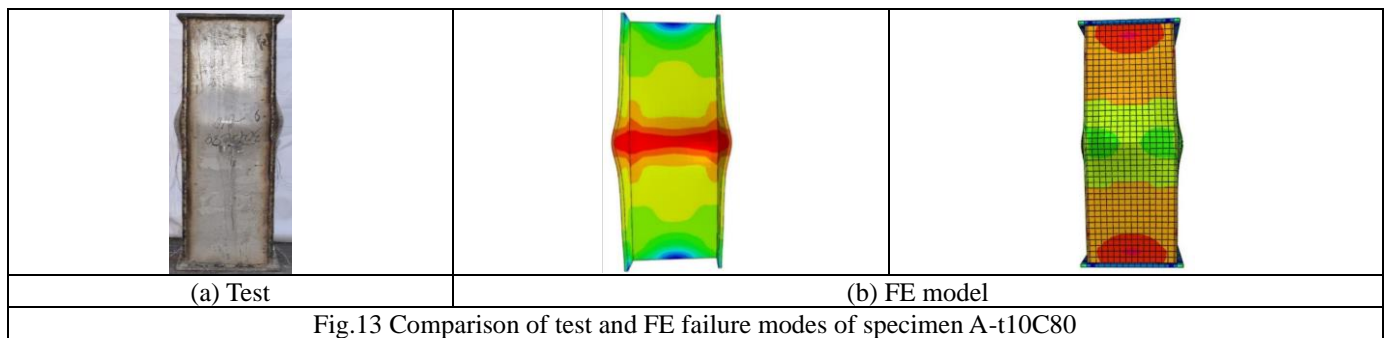
Table 5 Material properties and geometric dimensions considered in the parametric study

Steel grade	B (mm)	L (mm)	t (mm)	f_{cu} (MPa)	$\sigma_{0.2}$ (MPa)	E_0 (MPa)
304	200	600				
	300	900			205	1.93×10^5
	400	1200	8,10,12,14,16,18	40,45,50,55,60,70		
S32205	300	900				
	400	1200			450	2.00×10^5
	500	1500				

3.5 Model validation

Table 4 provides the comparison between test (N_{exp}) and FE (N_{FE}) ultimate loads for each specimen. The average N_{FE} to N_{exp} ratios of the austenitic and duplex CFSSST specimens are 1.04 and 1.06 with COV of 0.048 and 0.040, respectively. Comparisons between the test and FE load-axial deformation curves of typical austenitic and duplex CFSSST stub columns are given in Fig. 12, where good agreement between the test and FE curves can be observed. Figs. 13 and 14 show the test and the FE failure modes of Specimen A-t10C80 and Specimen D-t10C50, respectively, where in both cases the local buckling occurred in the test was accurately captured by the corresponding numerical model. In conclusion, the FE model developed can precisely duplicate the experimental results in regard to the ultimate resistance, load-axial deformation relationships and failure mode, and can be used in the subsequent parametric analysis.

4. Parametric study

4.1 Introduction

Upon the verification of the FE models developed in section 3, parametric analysis considering a wider range of material properties (i.e. concrete strengths) and geometric dimensions was carried out. The variables in the parametric study are detailed in Table 5, where two steel grades (austenitic 304 and duplex S32205 stainless steels), three cross-section outer widths, six tube wall thicknesses and six concrete strengths were considered, giving a total of 216 FE models generated. The key material properties used in the parametric analysis are given in Table 5.

4.2 Influence of steel tube slenderness

The influence of the stainless steel tube slenderness on the ultimate capacity of CFSSST stub columns is discussed in this section. To this end, selective sets of parametric results are plotted in Fig. 15, where the normalized load-deformation relationships of the austenitic specimens with $B = 300$ mm and $f_{cu} = 60$ MPa and duplex specimens with $B = 400$ mm and $f_{cu} = 60$ MPa are given. It can be found in Fig. 15 that as the stainless steel tube wall thickness increases from 8 to 18mm, the normalized peak load does not have a significant increase. However, the 'post-peak' performance of the load-displacement curve shown in Fig. 15 is indicated to be strongly associated with the wall

thickness (t). It can be due to the fact that the larger the tube thickness, the higher the residual bearing capacity from the steel after the concrete has been crushed.

4.3 Strength of concrete

To demonstrate the influence of the concrete strength on the bearing capacity of CFSSST specimens, normalized load-deformation curves of 304 t8-B200 and S32205 t8-B300 CFSSST specimens with varying concrete strengths are depicted in Fig. 16. It can be found in Fig. 16 that higher strength of concrete is associated with almost invariant normalized peak load and reduced normalized 'post-peak' resistance. This is mainly due to the fact that the contribution of concrete to the resistance after the ultimate load is almost the same regardless of the concrete grade, as illustrated in Fig. 17, where the load-deformation curves of the specimens in Fig. 16 are plotted. The peak load in these cases corresponded to the crushing of the concrete, after which the stainless steel tube buckled and displayed post buckling residual resistance which has no contribution from the crushed concrete.
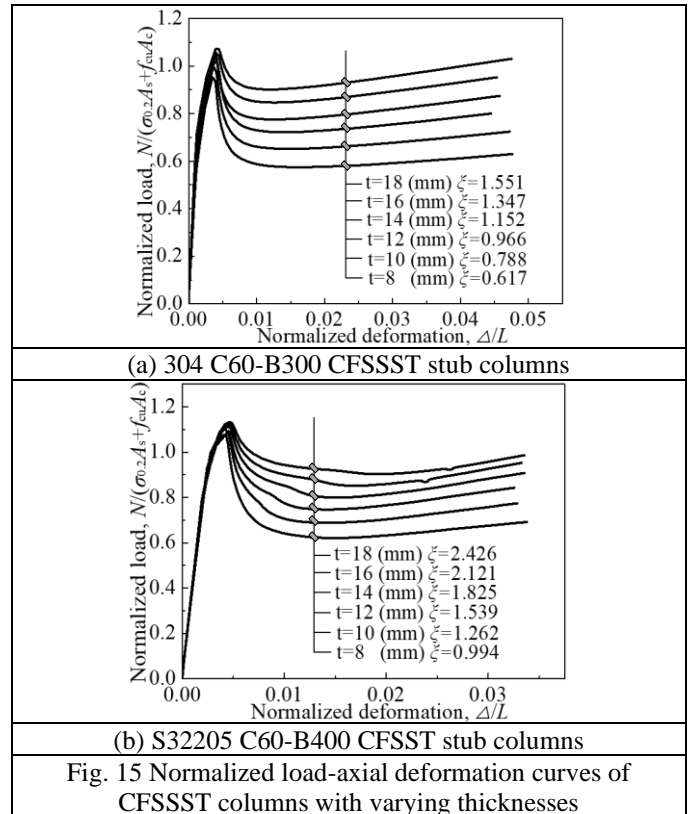

(a) 304 C60-B300 CFSSST stub columns

(b) S32205 C60-B400 CFSST stub columns

Fig. 15 Normalized load-axial deformation curves of CFSSST columns with varying thicknesses

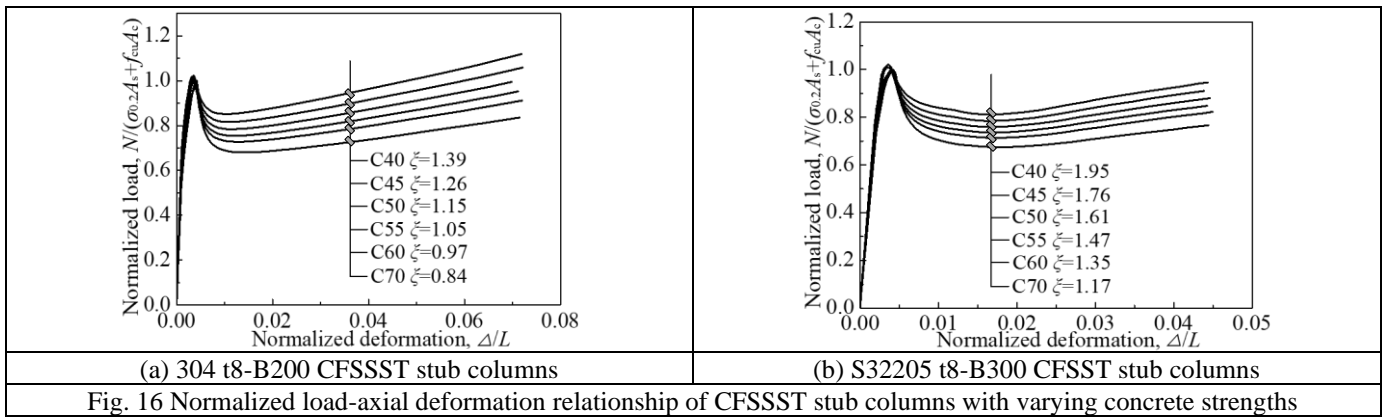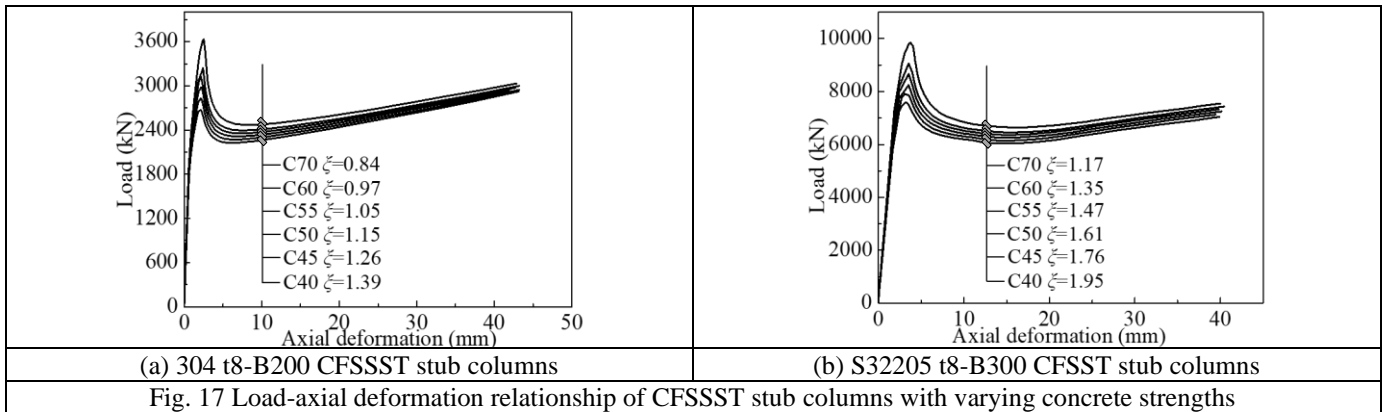| (a) 304 t8-B200 CFSSST stub columns	(b) S32205 t8-B300 CFSST stub columns
Fig. 16 Normalized load-axial deformation relationship of CFSSST stub columns with varying concrete strengths	

(a) 304 t8-B200 CFSSST stub columns	(b) S32205 t8-B300 CFSST stub columns
Fig. 17 Load-axial deformation relationship of CFSSST stub columns with varying concrete strengths	

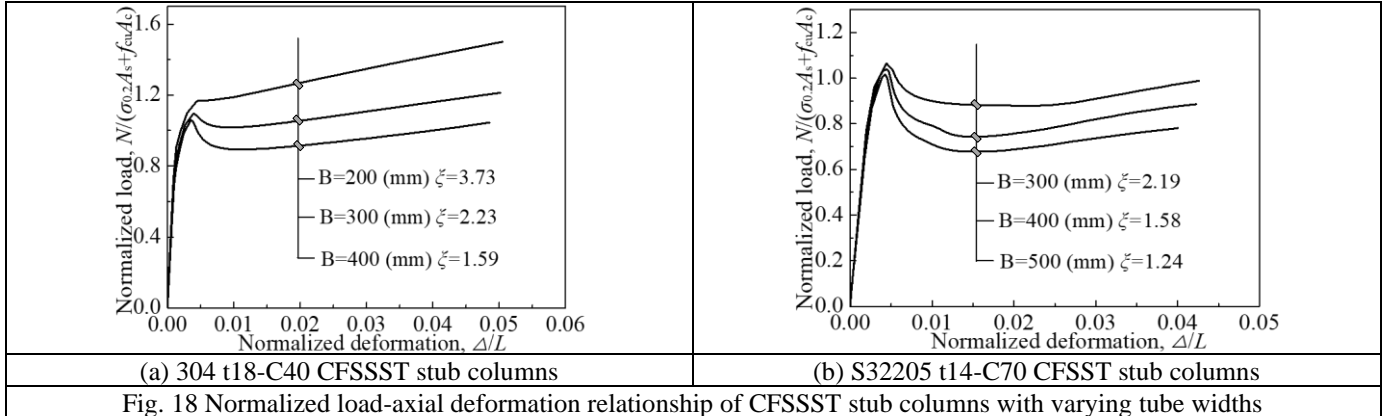| (a) 304 t18-C40 CFSSST stub columns	(b) S32205 t14-C70 CFSSST stub columns
Fig. 18 Normalized load-axial deformation relationship of CFSSST stub columns with varying tube widths	

4.4 The confinement factor ξ

The confinement factor $\xi = A_s f_{0.2}/A_c f_{ck}$ reflects the restraint of steel tube to concrete. Based on previous studies (Uy *et al.* 2011, Yang and Ma 2013), square tubes impose less confinement on concrete core compared with circular tubes as in the square tubes the confinement is mainly distributed at the corner regions. In addition to Figs. 15 and 16 where the confinement factors of each curves are specified, Fig. 18 compares the normalized load-displacement curves of CFSSST specimens with different cross-section widths with different confinement factors. It can be seen from Figs. 15, 16 and 18 that the influence of the confinement factors on the normalized peak load is not significant, although in general higher ξ are associated with slightly higher normalized peak loads. However, Figs. 15,

16 and 18 show clearly that the larger the confinement factor ξ, the higher the normalized residual capacity (post-peak strain-hardening behavior) of the CFSSST stub columns, as the contribution from the steel ($A_s f_{0.2}$) is higher in specimens with high confinement factors.

5. Assessment of existing design methods and proposed calculation methods

5.1 Introduction

Currently, there is no design guidance available to calculate the ultimate resistance under axial compression of CFSSST stub columns. However, design methods for conventional CFST are available in the North American

design guides, ACI 318 (2011) and ANSI 360/AISC (2010), the European standard, BS EN 1994-1-1 (2004) and the Chinese code, GB 50936 (2014). In this section, these design methods are examined against the experimental and FE results from the current research to assess their applicability on CFSSST members. In order to compare the different specifications, all material property values have been used as their characteristic values.

The North American design guidances ACI 318 (2011) and ANSI 360/AISC (2010) recommend that the ultimate resistance of the stub columns is the sum of the axial resistances of the concrete and the steel tube cross-sections, with a reduction coefficient applied to the concrete resistance to consider the effects of the cross-section slenderness. The reduction factor in ACI 318 (2011) is 0.85 for concrete filled square hollow section tube members, while ANSI/AISC 360 (2010) adopts different reduction factors according to the cross-section slenderness (e.g. compact, non-compact and slender). The specimens considered in the current study are all classified as 'compact', and the reduction factor specified by ANSI/AISC 360 (2010) for these specimens is the same as that of ACI 318 (2011), with a reduction factor of 0.85. Therefore, the bearing capacity (N_{US}) of CFST members in both design standards can be expressed as:

$$N_{US} = A_s f_y + 0.85 A_c f_c^{'} \qquad (6)$$

where f_y is the yield strength of the steel, with the 0.2% proof strength $f_{0.2}$ adopted herein for the stainless steel specimens considered in the current study.

The compressive design resistance N_{EC4} of square CFST stub columns specified in BS EN 1994-1-1 (2004) is given by Eq. (7), where the symbols are as defined previously.

$$N_{EC4} = A_s f_y + A_c f_c^{'} \qquad (7)$$

The GB 50936 (2014) calculates the bearing capacity of CFST stub columns based on the unified theory (Zhong 2006), which considers the steel tube and core concrete as a new composite material, with the resistance calculated as the 'composite' cross-sectional area A_{sc} times the 'composite' material strength f_{sc}, see Eq. (8). The 'composite cross-section area A_{sc} is defined as the sum of the A_s and A_c. The 'composite' material strength f_{sc} is associated with the confinement factor ξ and is specified according to the steel tube cross-section shape. For square hollow section CFST members, f_{sc} is calculated as in Eq. (9).

$$N_{GB} = A_{sc} f_{sc} \qquad (8)$$

$$f_{sc} = (1.212 + B\xi + C\xi^2) f_{ck} \qquad (9)$$

where B and C are factors specified as $B = 0.131 f_y/213 + 0.723$ and $C = -0.070\ f_{ck}/14.4 + 0.026$ for square hollow section CFST members.

5.2 ACI 318, ANSI/AISC 360 and EN 1994-1-1

The parametric analysis results and experimental results are compared with the predictions provided by the ACI 318 (2011) (Eq. 6) and BS EN 1994-1-1 (2004) (Eq. 7) methods in Figs. 19 and 20 for the 304 and S32205 CFSSST members, respectively. The average FE (test)-to-predicted

ultimate load ratio is also reported for each case in Figs. 19 and 20. The mean test-to-prediction ratios in brackets of Figs. 19 and 20 are all slightly higher than 1.0. Compared with the limited test data, the mean FE-to-prediction ratios in Figs. 19 and 20 are higher and the COV are smaller, indicating that both the ACI 318 (2011) (Eq. 6) and BS EN 1994-1-1 (2004) (Eq. 7) methods give conservative estimations of the resistances of CFSSST stub columns in both the austenitic and duplex stainless steel grades. This may be due to the fact that these codes do not consider the strain-hardening behavior of the stainless steel.
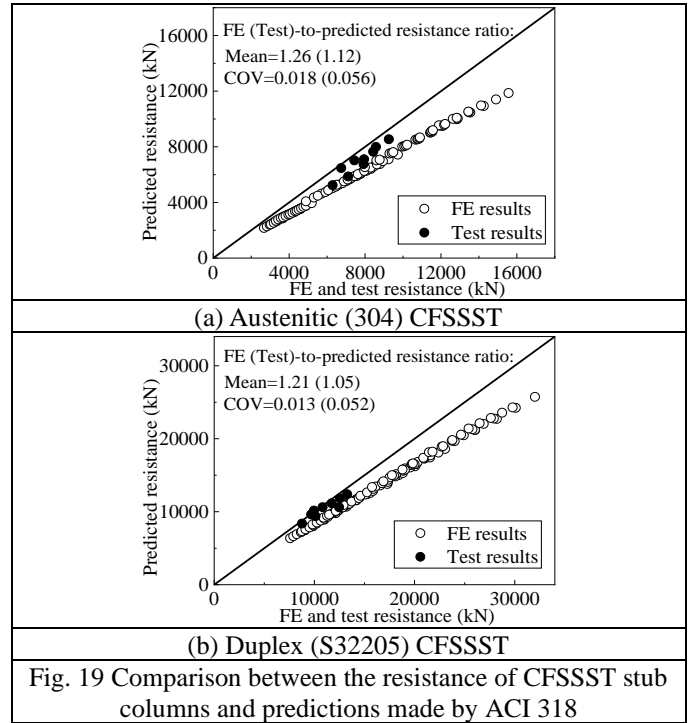

(a) Austenitic (304) CFSSST

(b) Duplex (S32205) CFSSST

Fig. 19 Comparison between the resistance of CFSSST stub columns and predictions made by ACI 318

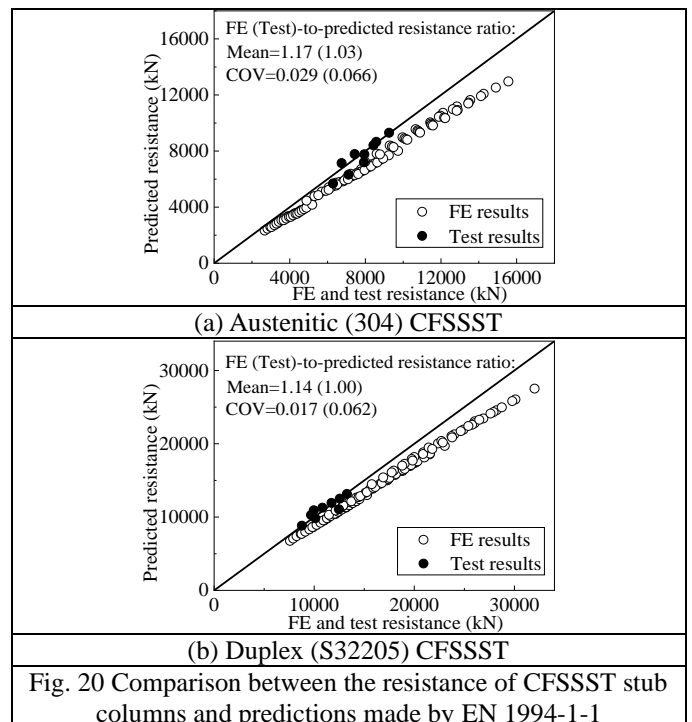(a) Austenitic (304) CFSSST

(b) Duplex (S32205) CFSSST

Fig. 20 Comparison between the resistance of CFSSST stub columns and predictions made by EN 1994-1-1

The Continuous Strength Method (CSM) (Afshan and Gardner 2013) is a newly deformation based design approach that has been further extended to steel-concrete composite structures (Gardner et al. 2017). It is recommended herein to replace the steel yield (0.2% proof) strength $f_{0.2}$ in Eqs. (6) and (7) with a failure strength σ_{csm} that considers the strain hardening behavior of stainless steel materials. The failure strength σ_{csm} can be obtained from the recently proposed CSM, where the cross-sectional resistance $A\sigma_{csm}$ is linked to its deformability (expressed according to the limiting strain, ε_{csm}), which has been observed to be associated with the cross-sectional slenderness $\bar{\lambda}_p$. The calculation of the σ_{csm} for the stainless steel tubes used in the current study should adopt the same procedure as established in Afshan and Gardner (2013). However, this is a rather complicated procedure to be used in practice.

To facilitate easy application, modifications to the ACI 318 (2011) and BS EN 1994-1-1 (2004) methods (Eqs. (6) and (7)) are proposed by applying a magnification factor, $\eta = \sigma_{csm}/f_{0.2}$, to increase the resistance contribution from the stainless steel tubes, leading to new expressions as given in Eqs. (10) and (11), respectively. In Eqs. (10) and (11), the magnification factors η for 304 and S32205 stainless steels were calculated by the FE results and an average value η_a is adopted for each grade, as given in Eq. (12). It should be noted that in Eqs. (10) and (11), a reduction factor ψ is also considered according to the recommendation by Lam and Gardner (2008), where it was found that simply replacing $f_{0.2}$ with σ_{csm} in design can lead to conservative predictions especially for CFSSST members with high concrete strengths. Therefore, the reduction factor was proposed as $\psi = (1 - f_c'/900)$ to reflect this phenomenon and to eliminate the strength overprediction of CFSSST stub columns with high concrete strengths. The new ACI 318 (2011) and BS EN 1994-1-1 (2004) predictions, denoted as $N_{US,mod}$ and $N_{EC4,mod}$, respectively, are compared with the test results of the current study in Table 6.

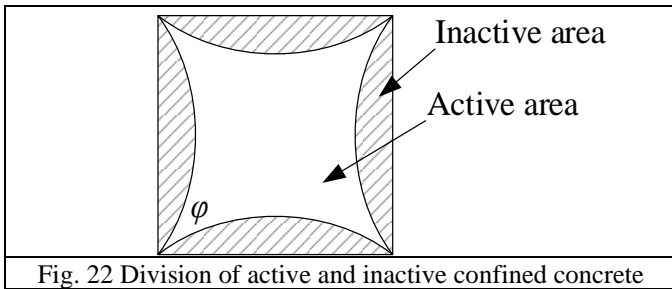|	
$N_{US,mod} = \psi(\eta_a A_s f_{0.2} + 0.85 A_c f_c')$	(10)
$N_{EC4,mod} = \psi(\eta_a A_s f_{0.2} + A_c f_c')$	(11)
$\eta_a = \begin{cases} 1.43 & \text{austenitic (304) CFSSST} \\ 1.16 & \text{duplex (S32205) CFSSST} \end{cases}$	(12)

Fig. 22 Division of active and inactive confined concrete

5.3 Assessment and modification to the GB 50936 design method

The results obtained from the parametric analysis and test are compared with the predictions made by the GB 50936 (2014) method (Eqs. (8) and (9)) in Fig 21. The mean FE (test)-to-predicted resistance ratios are 1.18 (1.04) and 1.22 (1.07) for the austenitic and duplex CFSSST specimens, respectively, indicating that GB 50936 generally provides conservative estimations for both the 304 and S32205 CFSSST stub columns.
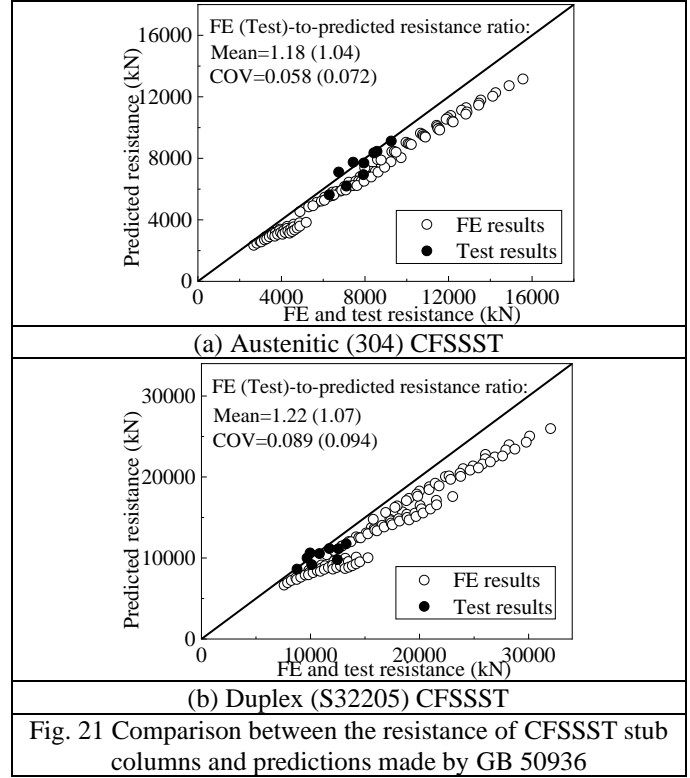

(a) Austenitic (304) CFSSST

(b) Duplex (S32205) CFSSST

Fig. 21 Comparison between the resistance of CFSSST stub columns and predictions made by GB 50936
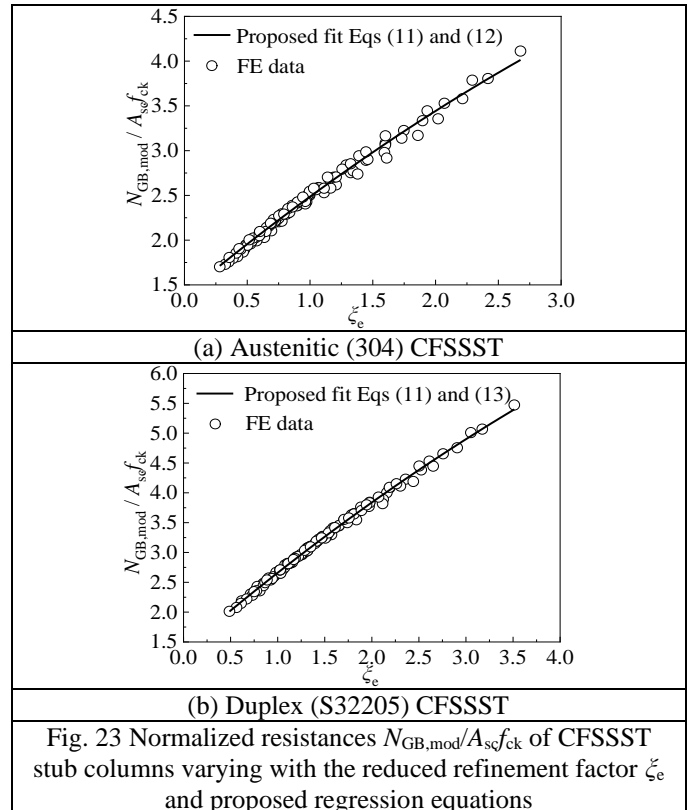

(a) Austenitic (304) CFSSST

(b) Duplex (S32205) CFSSST

Fig. 23 Normalized resistances $N_{GB,mod}/A_{sc}f_{ck}$ of CFSSST stub columns varying with the reduced refinement factor ξ_e and proposed regression equations

Table 6 Comparison between experimental and predicted results of CFSSST stub columns using modified calculation methods

Specimen label	N_{test} (kN)	$N_{US,mod}$ (kN)	$N_{EC4,mod}$ (kN)	$N_{GB,mod}$ (kN)	$N_{US,mod}/N_{test}$	$N_{EC4,mod}/N_{test}$	$N_{GB,mod}/N_{test}$
A-t8C50	6290	6010	6438	5856	0.96	1.02	0.93
A-t10C50	7113	6928	7357	6577	0.97	1.03	0.92
A-t12C50	7924	8143	8572	7480	1.03	1.08	0.94
A-t8C70	6743	7039	7664	7373	1.04	1.14	1.09
A-t10C70	7947	7938	8562	8145	1.00	1.08	1.02
A-t12C70	8575	9127	9751	9107	1.06	1.14	1.06
A-t8C80	7436	7483	8191	8003	1.01	1.10	1.08
A-t10C80	8430	8364	9072	8784	0.99	1.08	1.04
A-t12C80	9257	9536	10244	9760	1.03	1.11	1.05
Mean					1.01	1.09	1.02
COV					0.034	0.037	0.065
D-t8C50	8771	8921	9350	9203	1.02	1.07	1.05
D-t10C50	10111	10033	10462	10352	0.99	1.03	1.02
D-t12C50	12472	11399	11828	11725	0.91	0.95	0.94
D-t8C70	9686	9888	10513	10725	1.02	1.09	1.11
D-t10C70	10820	10977	11601	11948	1.01	1.07	1.10
D-t12C70	12560	12313	12937	13417	0.98	1.03	1.07
D-t8C80	9962	10300	11008	11333	1.03	1.10	1.14
D-t10C80	11728	11378	12085	12576	0.97	1.03	1.07
D-t12C80	13272	12701	13409	14071	0.96	1.01	1.06
Mean					0.99	1.04	1.06
COV					0.038	0.045	0.054

A few modifications to Eqs. (8) and (9) are proposed so as to improve the accuracy of the GB 50936 (2014) design method for CFSSST stub columns. The proposed GB 50936 (2014) design formulation is given in Eq. (13). The modifications include firstly a reduced confinement factor $\xi_e = k_e\xi$ to represent the reduced confined cross-sectional area of the concrete, as recommended by a previous study (Wu *et al.* 2017). The study suggests that the constraint of a square shaped tube to concrete is mainly concentrated at the corner regions and is poor at the flat regions, resulting in the division of active and inactive confined zones as illustrated in Fig. 22. It is recommended (Wu *et al.* 2017) that the confinement reduction factor k_e can be calculated as $k_e = 1-(2\tan\varphi)/3$, φ being initial tangent angle with a value of 23° for the square tube, giving $k_e = 0.717$. In addition, a reduction factor of $\psi = (1- f_c'/900)$, similar to that in section 5.2, is introduced to Eq. (13) to eliminate over-predictions when high concrete strengths are considered. Based on the new formulation of Eq. (13), regression analyses were performed to determine suitable A, B and C factors that provide the best fit to the obtained FE results, as illustrated in Fig. 23. The A, B and C factors for the austenitic (304) and duplex (S32205) CFSSST stub columns are given in Eqs. (14) and (15), respectively.

$$N_{GB,mod} = \psi A_{sc}(A + B\xi_e + C\xi_e^2)f_{ck}$$	(13)
A = 1.391, B = 1.162, C = -0.068 for austenitic (304) CFSSST	(14)
A = 1.363, B = 1.354, C = -0.058 for duplex (S32205) CFSSST	(15)

5.4 Formula validation

The results obtained from the test are listed in Table 6

and are compared with the predictions made by the modified American specifications (Eq. (10)), the modified BS EN 1994-1-1 (2004) (Eq. (11)) and modified GB 509356 (2014) (Eqs. (13) - (15)). The comparisons in Table 6 indicate that the proposals can well predict the compressive ultimate load of CFSSST stub columns with hot-rolled stainless steel tubes and the loads predicted by the modified American specifications are closer to the experimental results.

6. Conclusions

In this work, the axial resistance of CFSSST stub columns was investigated through a comprehensive test and FE program, which comprised of 18 CFSSST and 6 SHS tube tests and 234 FE model analyses. Based on the test and FE results, the following conclusions can be drawn:

• The failure modes for both the 304 and S32205 CFSSST stub columns appeared outwards (convex) local buckling waves in the steel tube, whereas the pure SHS specimens failed by typical inwards and outwards local buckling waves in adjacent steel plates. This indicates that in CFSSST specimens the tube has a restraining effect on the core concrete and the core concrete in turn affects the buckling mode of stainless steel tubes.

• The strain-hardening response of stainless steel tubes has a significant impact on post yielding resistance of CFSSST members, as indicated by the observation that the load-axial strain curves of austenitic CFSSST specimens possess significantly higher strain-hardening slopes than their duplex counterparts.

• The confinement factor does not significantly affect the normalized peak load (the load at which elastic range terminates) but higher confinement factor is

associated with higher post-yielding capacity of CFSST stub columns.

- Calculation methods developed based on the Continuous Strength Method and the design formula provided in ACI 318 and EN 1994-1-1 have been proposed for both hot-rolled austenitic and duplex CFSSST stub columns. Modifications to the GB 50936 design rules have also been proposed considering reduced confinement factors. The suitability of these proposals has been validated by comparison with the test results, where a good agreement between the predictions and the test results have been achieved.

Reference

ACI 318 (2011), Building code requirements for structural concrete, American Concrete Institute; Farmington Hills, MI, USA.

Afshan, S. and Gardner, L. (2013), "The continuous strength method for structural stainless steel design", *Thin-Walled Struct.*, **68**, 42-49. https://doi.org/10.1016/j.tws.2013.02.011

ANSI/AISC 360-10 (2010), Specification for structural steel buildings, American Institute of Steel Construction (AISC); Chicago, Illinois, USA.

ASTM A959 (2009), Standard guide for specifying harmonized standard grade compositions for wrought stainless steels, American Society for Testing and Materials; Pennsylvania, USA.

Averseng, J., Bouchair, A. and Chateauneuf, A. (2017), "Reliability analysis of the nonlinear behaviour of stainless steel cover-plate joints", *Steel Compos. Struct.*, **25**(1), 45-55. https://doi.org/10.12989/scs.2017.25.1.045

Baddoo, N.R. (2008), "Stainless steel in construction: a review of research, applications, challenges and opportunities", *J. Constr. Steel Res.*, **64**(11), 1199-1206. https://doi.org/10.1016/j.jcsr.2008.07.011

BS EN 1992-1-1 (2004), Design of concrete structures. Part 1-1: General rules and rules for buildings, European Committee for Standardization; Brussels, Belgium.

BS EN 1993-1-4 (2015), Design of steel structures. Part 1-4: General rules: supplementary rules for stainless Steels, European Committee for Standardization; Brussels, Belgium.

BS EN 1994-1-1 (2004), Design of composite steel and concrete structures. Part 1-1: General rules and rules for building, European Committee for Standardization; Brussels, Belgium.

BS EN ISO 6892-1 (2009), Metallic materials – Tensile testing. Part 1: Method of test at ambient temperature, The Standards Policy and Strategy Committee; London, UK.

Chen, Y., Feng, R. and Wang L. (2017), "Flexural behaviour of concrete-filled stainless steel SHS and RHS tubes", *Eng. Struct.*, **134**, 159-171. https://doi.org/10.1016/j.engstruct.2016.12.035

Chen, Z.P., Liu, X. and Zhou, W.X. (2018), "Residual bond behavior of high strength concrete-filled square steel tube after elevated temperatures", *Steel Compos. Struct.*, **27**(4), 509-523. https://doi.org/10.12989/scs.2018.27.4.509

Dai, P., Yang, L., Wang, J., Gang, Y. and Yang, S. (2019), "Experimental study on bearing behavior of concrete-filled square stainless steel tube stub columns under axial compression", *J. Build. Struct.* https://doi.org/10.14006/j.jzjgxb.2019.0595

Dai, P., Yang, L., Wang, J. and Zhou, Y. (2020), "Compressive strength of concrete-filled stainless steel tube stub columns", *Eng. Struct.*, **205**, 110106. https://doi.org/10.1016/j.engstruct.2019.110106

Ding, F.X., Yin, Y.X., Wang, L.P., Yu, Y.J., Luo, L. and Yu, Z.W. (2019), "Confinement coefficient of concrete-filled square stainless steel tubular stub columns", *Steel Compos. Struct.*, **30**(4), 337-350. https://doi.org/10.12989/scs.2019.30.4.337

Ellobody, E. and Young, B. (2006), "Design and behaviour of concrete-filled cold-formed stainless steel tube columns", *Eng. Struct.*, **28**(5), 716-728. https://doi.org/10.1016/j.engstruct.2005.09.023

Gardner, L., Saari, N. and Wang, F. (2010), "Comparative experimental study of hot-rolled and cold-formed rectangular hollow sections", *Thin-Walled Struct.*, **48**(7), 495-507. https://doi.org/10.1016/j.tws.2010.02.003

Gardner, L., Yun, X. Macorini. L. and Kucukler, M. (2017), "Hot-rolled steel and steel-concrete composite design incorporating strain hardening", *Structures*, **9**, 21-28. https://doi.org/10.1016/j.istruc.2016.08.005

Gao, X.F., Zhang, X.P., Liu, H.B., Chen, Z.H. and Li, H.Q. (2018), "Residual mechanical properties of stainless steels S30408 and S31608 after fire exposure", *Constr. Build. Mater.*, **165**, 82-92. https://doi.org/10.1016/j.conbuildmat.2018.01.020

GB 50010-2010 (2010), Code for design of concrete structures, Ministry of Housing and Urban-Rural Development of the People's Republic of China; Beijing, China.

GB 50936-2014 (2014), Technical code for concrete filled steel tubular structures, Ministry of Housing and Urban-Rural Development of the People's Republic of China; Beijing, China.

Gunawardena, Y.K.R., Aslani, F., Uy, B., Kang, W.H. and Hicks, S. (2019), "Review of strength behaviour of circular concrete filled steel tubes under monotonic pure bending", *J. Constr. Steel Res.*, **158**, 460-474. https://doi.org/10.1016/j.jcsr.2019.04.010

Han, L.H., Yao, G.H. and Zhao, X.L. (2005), "Tests and calculations for hollow structural steel (HSS) stub columns filled with self-consolidating concrete (SCC)", *J. Constr. Steel Res.*, **61**(9), 1241-1269. https://doi.org/10.1016/j.jcsr.2005.01.004

Han, L.H., Chen, F., Liao, F.Y., Tao, Z. and Uy, B. (2013), "Fire performance of concrete filled stainless steel tubular columns", *Eng. Struct.*, **56**, 165-181. https://doi.org/10.1016/j.engstruct.2013.05.005

He, A., Wang, F.Y. and Zhao, O. (2019), "Experimental and numerical studies of concrete-filled high-chromium stainless steel tube (CFHSST) stub columns", *Thin-Walled Struct.*, **144**, 106273. https://doi.org/10.1016/j.tws.2019.106273

Huang, Z., Jiang, L.Z., Chen, Y.F., Luo, Y. and Zhou, W.B. (2018), "Experimental study on the seismic performance of concrete filled steel tubular laced columns", *Steel Compos. Struct.*, **26**(6), 719-731. https://doi.org/10.12989/scs.2018.26.6.719

Lam, D. and Gardner, L. (2008), "Structural design of stainless steel concrete filled columns", *J. Constr. Steel Res.*, **64**(11), 1275-1282. https://doi.org/10.1016/j.jcsr.2008.04.012

Li, Y.L., Zhao, X.L., Singh, R.K.R. and Al-Saadi, S. (2016), "Experimental study on seawater and sea sand concrete filled GFRP and stainless steel tubular stub columns", *Thin-Walled Struct.*, **106**, 390-406. https://doi.org/10.1016/j.tws.2016.05.014

Li, Y.L., Zhao, X.L., Singh, R.K.R. and Al-Saadi, S. (2016), "Tests on seawater and sea sand concrete-filled CFRP, BFRP

and stainless steel tubular stub columns", *Thin-Walled Struct.*, **108**, 163-184. https://doi.org/10.1016/j.tws.2016.08.016

Liao, F.Y., Han, L.H., Tao, Z. and Rasmussen, K.J.R. (2017), "Experimental behavior of concrete-filled stainless steel tubular columns under cyclic lateral loading", *J. Struct. Eng. ASCE*, **143**(4), 04016219. https://doi.org/10.1061/(ASCE)ST.1943-541X.0001705

Mirambell, E. and Real, E. (2000), "On the calculation of deflections in structural stainless steel beams: an experimental and numerical investigation", *J. Constr. Steel Res.*, **54**(1), 109-133. https://doi.org/10.1016/S0143-974X(99)00051-6

Qu, X.S., Chen, Z.H., Nethercot, D.A., Gardner, L. and Theofanous, M. (2015), "Push-out tests and bond strength of rectangular CFST columns", *Steel Compos. Struct.*, **19**(1), 21–41. https://doi.org/10.12989/scs.2015.19.1.021

Ramberg, W. and Osgood, W.R. (1943), "Description of stress-strain curves by three parameters", Tech. Report No. 902; Nat. Advisory Committee for Aeronautics, Washington, D.C., USA.

Rasmussen, K.J.R. (2003), "Full-range stress–strain curves for stainless steel alloys", *J. Constr. Steel Res.*, **59**(1), 47-61. https://doi.org/10.1016/S0143-974X(02)00018-4

Rossi, B. (2014), "Discussion on the use of stainless steel in constructions in view of sustainability", *Thin-Walled Struct.*, **83**, 182-189. https://doi.org/10.1016/j.tws.2014.01.021

Sakino, K., Nakahara, H., Morino, S. and Nishiyama, I. (2004), "Behavior of centrally loaded concrete-filled steel-tube short columns", *J. Struct. Eng. ASCE*, **130**(2), 180-188. https://doi.org/10.1061/(ASCE)0733-9445(2004)130:2(180)

Tam, V.W.Y., Wang, Z.B. and Tao, Z. (2014), "Behaviour of recycled aggregate concrete filled stainless steel stub columns", *Mater. Struct.*, **47**(1-2), 293-310. https://doi.org/10.1617/s11527-013-0061-1

Tao, Z., Song, T.Y., Uy, B. and Han, L.H. (2016), "Bond behavior in concrete-filled steel tubes", *J. Constr. Steel Res.*, **120**, 81-93. https://doi.org/10.1016/j.jcsr.2015.12.030

Tao, Z., Wang, Z.B. and Yu, Q. (2013), "Finite element modelling of concrete-filled steel stub columns under axial compression", *J. Constr. Steel Res.*, **89**, 121-131. https://doi.org/10.1016/j.jcsr.2013.07.001

Thomas, J. and Sandeep, T.N. (2018), "Experimental study on circular CFST short columns with intermittently welded stiffeners", *Steel Compos. Struct.*, **29**(5), 659-667. https://doi.org/10.12989/scs.2018.29.5.659

Uy, B., Tao, Z. and Han, L.H. (2011), "Behavior of short and slender concrete-filled stainless steel tubular columns", *J. Constr. Steel Res.*, **67**(3), 360-378. https://doi.org/10.1016/j.jcsr.2010.10.004

Wang, B., Liang, J.H. and Lu, Z. (2019), "Experimental investigation on seismic behavior of square CFT columns with different shear stud layout", *J. Constr. Steel Res.*, **153**, 130-138. https://doi.org/10.1016/j.jcsr.2018.10.004

Wang, L.P., Cao, X.X., Ding, F.X., Luo, L., Sun, Y., Liu, X.M. and Su, H.L. (2018), "Composite action of concrete-filled double circular steel tubular stub columns", *Steel Compos. Struct.*, **29**(1), 77-90. https://doi.org/10.12989/scs.2018.29.1.077

Wang, Z.B., Tao, Z., Han, L.H., Uy, B., Lam, D. and Kang, W.H. (2017), "Strength, stiffness and ductility of concrete-filled steel columns under axial compression", *Eng. Struct.*, **135**, 209-221. https://doi.org/10.1016/j.engstruct.2016.12.049

Wu, H.P., Qiao, Q.Y., Cao, W.L., Dong, H.Y. and Zhang, J.W. (2017), "Axial compressive behavior of special-shaped concrete filled tube mega column coupled with multiple cavities", *Steel Compos. Struct.*, **23**(6), 633-646. https://doi.org/10.12989/scs.2017.23.6.633

Yang, Y.F. and Ma, G.L. (2013), "Experimental behaviour of recycled aggregate concrete filled stainless steel tube stub columns and beams", *Thin-Walled Struct.*, **66**, 62-75. https://doi.org/10.1016/j.tws.2013.01.017

Young, B. and Ellobody, E. (2006), "Experimental investigation of concrete-filled cold-formed high strength stainless steel tube columns", *J. Constr. Steel Res.*, **62**(5), 484-492. https://doi.org/10.1016/j.jcsr.2005.08.004

Zhao, Y.S. (2013), "Summary of the development on concrete filled steel tube structure", *2nd International Conference on Civil Engineering and Transportation (ICCET 2012)*, Guilin, China, October.

Zhong, S.T. (2006), *Unified Theory of Concrete Filled Steel Tube: Research and Application*, Tsinghua University Press, Beijing, China.